

Article

# Face with Mask Detection in Thermal Images Using Deep Neural Networks

Natalia Głowacka \*  and Jacek Rumiński 

Department of Biomedical Engineering, Faculty of Electronics, Telecommunications and Informatics, Gdansk University of Technology, Narutowicza 11/12, 80-233 Gdansk, Poland; jacek.ruminski@pg.edu.pl

\* Correspondence: natalia.glowacka@pg.edu.pl

**Abstract:** As the interest in facial detection grows, especially during a pandemic, solutions are sought that will be effective and bring more benefits. This is the case with the use of thermal imaging, which is resistant to environmental factors and makes it possible, for example, to determine the temperature based on the detected face, which brings new perspectives and opportunities to use such an approach for health control purposes. The goal of this work is to analyze the effectiveness of deep-learning-based face detection algorithms applied to thermal images, especially for faces covered by virus protective face masks. As part of this work, a set of thermal images was prepared containing over 7900 images of faces with and without masks. Selected raw data preprocessing methods were also investigated to analyze their influence on the face detection results. It was shown that the use of transfer learning based on features learned from visible light images results in mAP greater than 82% for half of the investigated models. The best model turned out to be the one based on Yolov3 model (mean average precision—mAP, was at least 99.3%, while the precision was at least 66.1%). Inference time of the models selected for evaluation on a small and cheap platform allows them to be used for many applications, especially in apps that promote public health.

**Keywords:** thermal images; face detection; face with mask detection; deep neural networks



**Citation:** Głowacka, N.; Rumiński, J. Face with Mask Detection in Thermal Images Using Deep Neural Networks. *Sensors* **2021**, *21*, 6387. <https://doi.org/10.3390/s21196387>

Academic Editor: Italo Zoppis

Received: 22 August 2021  
Accepted: 22 September 2021  
Published: 24 September 2021

**Publisher's Note:** MDPI stays neutral with regard to jurisdictional claims in published maps and institutional affiliations.



**Copyright:** © 2021 by the authors. Licensee MDPI, Basel, Switzerland. This article is an open access article distributed under the terms and conditions of the Creative Commons Attribution (CC BY) license (<https://creativecommons.org/licenses/by/4.0/>).

## 1. Introduction

Face detection in thermal images using deep neural networks is still a challenge because of small amount of thermal images needed for algorithms learning. The biggest advantages of using the thermal domain is possibility of detecting during night and day and independence from weather and illumination condition. The advantages of using thermal images are used, among others, for face detection and tracking [1], face recognition [2], analysis of local temperature changes [3,4] or estimation of biomedical signals [5,6]. Low resolution thermal cameras become more available and the features obtained from such thermal images can be improved using deep-learning-based algorithms such as super-resolution algorithms [7] or transformers [8]. The use of thermal imaging in conjunction with deep learning, using available and cheap thermographic cameras and small modules containing GPU, will allow quickly analyzing images and create low-cost systems, for example for remote health control.

### 1.1. Literature Review

There are some algorithms developed primarily for face detection in thermal images—Projection Profile Analysis (PPA) [9] or Eye Corner Detection (ED) [10]. These algorithms are well suited for detecting in images where the person is dominant object in the image and its whole head and upper part of torso are visible.

In computer vision tasks, face detection is one of basic, the most popular and well known issue. In visible light images spectrum are a lot of solutions for this task, including many of them are based on deep neural networks. Of course, there are also traditional solutions, including Viola-Jones [11], but now classical methods are often replaced by newer

solutions based on deep learning. Zhang et al. [12] designed face detector named FaceBoxes. This convolutional neural network model was created to have superior performance on both speed and accuracy. The speed of FaceBoxes is unchanging to the number of faces in the picture. It achieves a good accuracy in comparing with another face detection methods. Face detection can also be performed on the basis of well-known models designed for object detection. Yang and Jiachun [13] applied YOLO model to face detection. The model was trained on WIDER FACE data set [14]. Using YOLO the speed of detection can meet real-time detection requirements. From the other side, face detection can be performed in conjunction with a face recognition task. This multi-task solution was used in F-DR Net [15]. F-DR Net has a parallel architecture and detection network based on FaceBoxes model. This method was evaluated on several face detection and recognition datasets and it has better recognition and detection accuracy than other methods. Several deep-learning-based approaches focused on face and face mask detection have been investigated in [16]. The study was based on visible light images demonstrating high classification accuracy using the fine-tuned VGG-16 model.

For face detection in thermal images, such as in the visible spectrum, algorithms or machine learning-based approaches can be used. In [17], authors compare five algorithms which have been successfully applied for face detection in visible light images with algorithms especially designed for detection in thermal images. The Haar cascade classifier [11], Histograms of Oriented Gradients (HOG) [18] and the other can be used for detection in thermal images if trained with a well-fitting database. On the other hand, when deep neural networks are more efficient, it is naturally to use this solution for face detection. Attempts to adapt the neural networks used with visible light images have brought many successes. One of the models commonly used for face detection in thermal imaging is Yolov3 [19]. This model was made for object detection and its most salient feature is making detection at three different scales—small objects can be well detected because of preserving the fine grained features. Yolov3 was adopted for face detection in thermal images for in-vehicle monitoring of passengers in [20]. The results of authors experiments on their test set show an  $AP_{50}$  of 99.7% and an AP of 78.5%. In [1], the authors analyze using deep learning algorithms for face detection in low resolution thermal sequences. The Inception v3 model [21] was used—it is a great model for object classification, but it was trained on visible light images. To resolve this problem, transfer learning technique can be used for re-training the Inception v3. The model returns only class probabilities, so its last layer should be modified for object detection task. The changes introduced to the model allowed it to be successfully adapted to detection on thermal images. Thermographic images are also used for tasks other than face detection. Peng et al. in [22] created NIRFaceNet—a convolutional neural network modified from GoogLeNet [23]. It has fewer parameters than previously designed AlexNet [24], but model achieving higher accuracy. The experimental results compared to other solutions—such as Local Binary Pattern + Principal Component Analysis (LBP + PCA) [25] or GoogLeNet, demonstrate that the proposed architecture has an overall advantage, especially when image has blur or noise. In the other hand, thermal images are used for face authentication [26]. The proposed neural network architecture consists of 12 sequential layers, which takes as input one channel image. The data set used includes faces in different positions, lightning conditions and emotions, that gives the model the ability to recognize in any condition. In compared to state-of-the-art thermal face recognition algorithms (like NIRFaceNet or GoogLeNet), the proposed method achieves better recognition accuracy (99.6%). Another algorithm created for thermal face recognition tasks was made by Wu et al. [2]. Proposed model optimizes the neural network structure through the local receptive field, power sharing and sampling. Using the RGB-D-T face database [27] for CNN testing and comparing with other methods such as LBP, HOG in categories: head rotation, expression, and illumination are conditions. In all categories, the method created by us has the best thermal recognition accuracy.

## 1.2. Contribution

In this paper, we explored whether and how the face detection algorithms designed for detecting in visible light can be adapted for thermal images of a face with and without a virus protective mask work. We analyzed four face detection algorithms with different base models using about 8000 thermal images that we collected with four different thermal cameras. Additionally, we analyzed the role of different thermal raw data preprocessing methods on face detection quality metrics. We check whether using a cheap and small module equipped with a GPU, it is possible to achieve a satisfactory inference time for use in everyday applications (e.g., for remote temperature control). Finally, we investigated the role of transfer learning using features learned on visible light images.

## 2. Materials and Methods

Due to the lack of access to a large number of thermal images of the face especially with virus protective masks, we decided to create our own image database. The database contains thermal images of the face and their descriptions (location in the image and information on whether the person wear face mask, face visor or be without them). The experiment was performed with permission of local Committee for Ethics of Research with Human Participants of 02.03.2021.

### 2.1. Description of Cameras

Thermal sequences were collected using several cameras to obtain more varied dataset. The descriptions of used cameras are shown below in Table 1.

**Table 1.** Descriptions of cameras.

Model	Manufacturer	Spatial Resolution	Dynamic Range	Frame Rate
A320G	FLIR Systems	320 × 240	16 bit	60 fps
A655SC	FLIR Systems	640 × 480	16 bit	50 fps
SC3000	FLIR Systems	320 × 240	14 bit	50 fps
Boson	FLIR Systems	640 × 512	14 bit	8 fps

### 2.2. Image Acquisition Methods

Using various types of cameras, we recorded thermal sequences from which individual images was extracted. These sequences depicts people who's entering the building (these people should wear different types of masks, but also can be without them), people moving towards the camera, and the faces of people with and without a mask making head movements (a side-to-side and an up-and-down movements) at two different distances from the cameras (60 cm and 250 cm). Due to different types of recordings, the faces shown in the pictures are in different positions and in different scales. Recorded thermal sequences contain both good and poor quality images. Examples of such images are shown in Figure 1.

### 2.3. Dataset

The dataset consisted of 7920 images. It contains 7285 images where people are wearing a mask and 635 images where people are without one. The created dataset is not balanced, because we were interested in images with masks and images without masks only for reference. The entire dataset includes 10,555 face labels, since some images had more than one face. Among the collected images, women accounted for 42% of participants in the experiment, and men for 58%. The average age of people was 26.42 years. The created dataset was divided into training (90%) and test sets (10%). The test set includes images captured by each camera and images with and without masks.

From test set we extracted two smaller sets—one containing images with mask and second containing images without. The first one include 6% of collected images and the second one—4%. After that, we obtained three test sets—original, with mask and without mask.



**Figure 1.** Examples of two types of images included in dataset: (a) good quality image and (b) poor quality image.

#### 2.4. Annotations of Images

After collecting thermal sequences, we extract some frames of every sequences. For FLIR A655SC and SC3000 frame offset was set to 20 (which means that every 8th frame was annotated), for FLIR Boson to 10 and for FLIR A320G to 8. To describe them, we have created a web application that allows to create annotations, which was based on websocket technology. For showing frames from a sequence, every frame was converted using normalization to 0–255 range, next saved as grayscale image and shown during annotation. For each frame, the description includes the location of each faces in the image and information whether a face mask (or face visor) is or not on the face. The criteria for annotating the face were: marking the regions with rectangles that include the forehead, the chin and the cheeks, and a region could be marked if a minimum of 50% of its area and two eyes were visible. When describing the images, if the annotator was unsure that the face mask was on, it should mark that the person has not it on the face. Additionally, to mark the region with ‘face mask’ label, the face mask should cover at least mouth. Annotation of images was made by eight people. Face is relatively easy to recognize by the experts, so we assume that annotations of faces were done correctly.

#### 2.5. Data Preprocessing

Recorded sequences were saved as raw data. This type of saving sequences allows for extensive preprocessing of data that will be used for model training and testing. The first step is to normalize the entire range of raw data values to 0–255 for each frame. The second version of data preprocessing is to change the contrast of images using Contrast Limited Adaptive Histogram Equalization with 8x8 window. This type of histogram equalization is added to images with original values range of raw data, which are next normalize to 0–255 range (like in first type). The last one type of image preprocessing is to use image colorization to the images in dataset. All of analyzed algorithms were designed to work with images registered in visible light. Image colorization of thermal images should increase accuracy achieved by the models. It was done with the use of a solution proposed by the authors of the article [28]. An example of three data preprocessing cases are shown in Figure 2.

Due to the use of three different data preprocessing methods, the original test set was also presented in three versions: original (normalized), with CLAHE and with colorization.



**Figure 2.** Example of three types of preprocessing: (a,b) images with normalized range of raw data, (c) image is image (a) after changing contrast using CLAHE and (d) image is image (b) after colorization.

### 2.6. Adaptation of Deep Learning Models

We have decided to analyze four deep learning face detection models with different base models, which originally was designed to detect faces in visible light images. This will allow us to analyze the effectiveness of deep-learning-based face detection algorithms applied to thermal images, especially for faces covered by virus protective face masks.

First of chosen models is UltraLight model [29]. This model was designed for face detection and for being lightweight for using in edge computing devices. The authors provided two versions of model: version-slim (with network backbone simplification, slightly faster) and version-RBF (with the modified RFB module and higher precision). The size of the model is approximately 1MB. For these two versions, the hyperparameters were the same and are listed in Table 2. For this model, learning rate was reduced by 0.1 after 95 and 150 epoch.

**Table 2.** Models hyperparameters.

Model Name	Base Model	Number of Epochs	Batch Size	Optimizer	Initial Learning Rate
UltraLight	version-slim version-RBF	200	24	SGD	0.01
RetinaFace	MobileNet-0.25	250	32	SGD	0.001
	ResNet-50	200	24		
Yolov3	-	200	16	SGD	0.01
LFFD	-		32	SGD	0.1

RetinaFace [30] is the second model selected for testing. This model was originally created using Mxnet library, but we use its implementation in PyTorch [31]. The authors provided two versions of backbone net—MobileNet-0.25 and ResNet-50. Base models hyperparameters are shown in Table 2 below. The models was trained using SGD as optimization method with 0.9 momentum, weight decay at 0.0005. Initial learning rate was

divided by 10 at 190 and 220 epoch in Mobilenet-0.25 version and at 150 and 190 epoch in ResNet-50 version.

The next one was the Yolov3 model [19]. Before starting the selection of the type of Yolo model, preliminary tests for thermal images were carried out between versions: 3, 4, and 5. As the best results were obtained for the Yolo model in version 3, it was selected for analysis. Its implementation in PyTorch was used. The optimization method is SGD with 0.937 Nesterov momentum and 0.0005 weight decay. The remaining model hyperparameters are included in Table 2. At the beginning of the training process, a warm-up (3 epochs) is performed. The learning rate is changed with cosine function.

LFFD: A Light and Fast Face Detector for Edge Devices [32] was the last selected for testing. This detector balancing both accuracy and running efficiency. The testing task will use the second version (v2) of the model (not presented in the article). In this version, detection scale is 10–320 and the backbone is modified for faster inference compared to the version presented in the paper. SGD with 0.9 momentum was used as optimization method and 0.00001 weight decay. The model was trained over 1,000,000 iterations, and the learning rate was reduced by dividing by 10 the current value at the 300,000, 600,000 and 900,000th iterations.

Each model additionally introduces its own image preprocessing. The Yolov3 model uses a random change of perspective and random changes in color, hue, saturation, and brightness. The LFFD model also uses random changes in saturation and brightness, but also in contrast, random horizontal and vertical flip, and blur. Classic preprocessing, like brightness, contrast, saturation, and hue random changes, is used by RetinaFace too. In addition, image cropping, mirroring or resizing to a given dimension are also used. The last model—the Ultra Light model—uses the same methods as in the RetinaFace model, but also randomly adds noise to the image.

### 2.7. Models Testing Scenario

We decided to carry out two different approaches to testing selected models. Figure 3 shows the framework model of the testing scenario. The first approach was to see how each model performs face detection in thermal images when it was trained on the visible images dataset. In our case it was the WIDER FACE dataset for all models. The second approach involves the use of already acquired knowledge while training models on a set of visible images—transfer learning. In this case, we use a model that has already been trained and we fine-tuned it using the database created by us. The use of transfer learning consists of taking a model previously trained on a set of visible images (in our case on WIDER face database), then we use freezing the layers of the basic model and train the last layers to adapt model to work with thermal images.

For each of the approaches, each model will be evaluated on the three created test sets.

The last element of the evaluation of selected models will be to measure the inference time to check if it is satisfactory enough to use the models in applications in everyday life. The inference time will be measured for images with two resolutions— $640 \times 480$  and  $320 \times 240$  pixels, using the NVIDIA Jetson Nano module (with NVIDIA Maxwell architecture) and DGX-1 station (on one NVIDIA Tesla V100 SXM2 32GB GPU).

### 2.8. Metrics

To measure the performance of the analyzed models we have choose three metrics: mean Average Precision (mAP) [33], precision, and recall [34]. They are a popular metrics for measuring accuracy of object detectors. Precision measures accuracy of predictions (percentage of correct predictions), while recall measures the number of correct positive prediction in all positive prediction. Average precision combines precision and recall (calculating the area under the curve (AUC) of the Precision x Recall curve) and the higher the score is, the higher performance the model has.

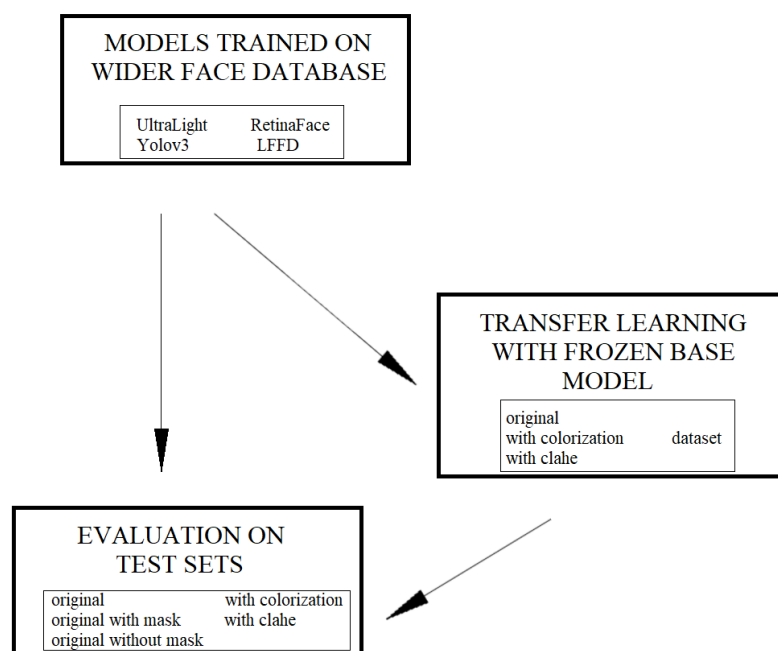


**Figure 3.** The framework model of the testing scenario.

### 3. Results

Tables 3–6 show the results obtained for each test scenario. The results obtained for each model and test set are the average of three test approaches in order to avoid randomness of the obtained results. The use of models learned only on images recorded in visible light does not give particularly high and desirable results in the case of thermal images. Compared to other models, the Yolov3 model is distinguished by a particularly high value of the mean average precision (mAP), precision, and recall. Moreover, for the remaining models, the collected metrics for the original test set with faces only in masks were significantly lower than for the mixed sets, and for the set with images of faces without masks, they reached the highest values.

**Table 3.** Results obtained for testing model trained on WIDER FACE dataset.

Trained on WIDER FACE				
Model	Dataset	mAP	Precision	Recall
UltraLight	original	0.165	0.514	0.144
	with CLAHE	0.207	0.514	0.196
	with colorization	0.216	0.530	0.209
	original with mask	0.107	0.436	0.105
	original without mask	0.267	0.598	0.210
	original	0.166	0.514	0.180
	with CLAHE	0.200	0.535	0.192
	with colorization	0.222	0.539	0.260
	original with mask	0.096	0.398	0.121
	original without mask	0.286	0.640	0.281

Table 3. Cont.

Trained on WIDER FACE				
Model	Dataset	mAP	Precision	Recall
RetinaFace	original	0.315	0.565	0.285
	with CLAHE	0.337	0.594	0.297
	with colorization	0.296	0.475	0.325
	original with mask	0.218	0.487	0.209
	original without mask	0.467	0.648	0.416
	original	0.233	0.464	0.245
	with CLAHE	0.274	0.528	0.261
	with colorization	0.231	0.434	0.254
	original with mask	0.125	0.353	0.172
	original without mask	0.392	0.597	0.373
Yolov3	original	0.994	0.638	0.997
	with CLAHE	0.996	0.634	0.997
	with colorization	0.996	0.621	0.997
	original with mask	0.994	0.625	0.998
	original without mask	0.994	0.663	0.996
LFFD	original	0.163	0.461	0.168
	with CLAHE	0.220	0.562	0.206
	with colorization	0.172	0.439	0.193
	original with mask	0.090	0.360	0.119
	original without mask	0.287	0.570	0.252

The use of transfer learning has shown satisfactory results for the UltraLight, LFFD, and RetinaFace models. Using the original training set, the best results are achieved by the Ultra Light model, comparable for the slim and RBF versions. When the contrast enhanced image set using CLAHE was selected as the training set, in addition to the Yolov3 model, the Ultra Light model performs well with face recognition, especially for the RBF version, where the mAP is over 80%. The use of the training set with CLAHE, compared to the basic, original training set, resulted in an improvement of the mAP metric for the RetinaFace model—using the MobileNet model and for the Ultra Light model in the RBF version.

Table 4. Results obtained for testing model trained on own original dataset.

Transfer Learning—Original Training Set				
Model	Dataset	mAP	Precision	Recall
UltraLight version-slim	original	0.839	0.802	0.829
	with CLAHE	0.795	0.788	0.749
	with colorization	0.828	0.799	0.829
	original with mask	0.836	0.793	0.834
	original without mask	0.844	0.820	0.822



Table 4. Cont.

Transfer Learning—Original Training Set				
Model	Dataset	mAP	Precision	Recall
version-RBF	original	0.829	0.826	0.819
	with CLAHE	0.764	0.818	0.713
	with colorization	0.836	0.835	0.818
	original with mask	0.831	0.810	0.826
	original without mask	0.827	0.855	0.807
MobileNet-0.25	original	0.473	0.674	0.444
	with CLAHE	0.347	0.543	0.353
	with colorization	0.399	0.655	0.375
	original with mask	0.333	0.577	0.352
	original without mask	0.662	0.798	0.609
RetinaFace	original	0.516	0.755	0.515
	with CLAHE	0.435	0.655	0.478
	with colorization	0.474	0.721	0.496
	original with mask	0.437	0.703	0.433
	original without mask	0.618	0.823	0.654
Yolov3	original	0.996	0.716	0.997
	with CLAHE	0.994	0.727	0.997
	with colorization	0.996	0.718	0.997
	original with mask	0.996	0.691	0.998
	original without mask	0.993	0.764	0.996
LFFD	original	0.688	0.748	0.667
	with CLAHE	0.608	0.743	0.555
	with colorization	0.685	0.753	0.659
	original with mask	0.722	0.749	0.715
	original without mask	0.645	0.743	0.585

Table 5. Results obtained for testing model trained on own dataset with CLAHE.

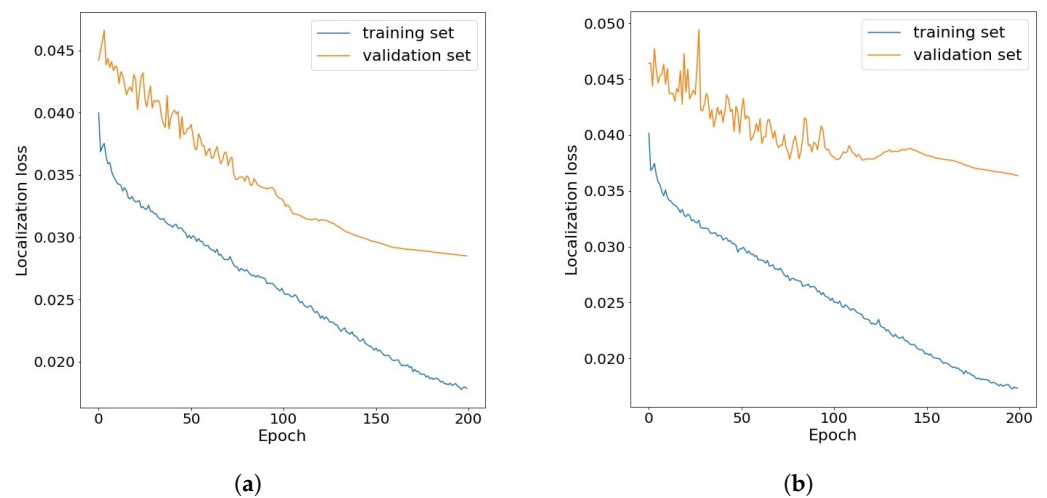
Transfer Learning—Training Set with CLAHE				
Model	Dataset	mAP	Precision	Recall
UltraLight version-slim	original	0.780	0.805	0.778
	with CLAHE	0.780	0.802	0.794
	with colorization	0.771	0.803	0.775
	original with mask	0.795	0.805	0.792
	original without mask	0.759	0.803	0.758

Table 5. Cont.

Transfer Learning—Training Set with CLAHE				
Model	Dataset	mAP	Precision	Recall
version-RBF	original	0.843	0.852	0.770
	with CLAHE	0.843	0.839	0.786
	with colorization	0.823	0.847	0.741
	original with mask	0.840	0.840	0.771
	original without mask	0.850	0.872	0.776
MobileNet-0.25	original	0.506	0.704	0.472
	with CLAHE	0.507	0.700	0.476
	with colorization	0.494	0.716	0.437
	original with mask	0.386	0.622	0.385
	original without mask	0.675	0.805	0.623
RetinaFace	original	0.469	0.729	0.494
ResNet-50	with CLAHE	0.565	0.767	0.562
	with colorization	0.438	0.745	0.450
	original with mask	0.385	0.666	0.416
	original without mask	0.605	0.815	0.629
	original	0.994	0.727	0.997
Yolov3	with CLAHE	0.995	0.725	0.997
	with colorization	0.994	0.731	0.997
	original with mask	0.994	0.711	0.998
	original without mask	0.994	0.761	0.996
	original	0.511	0.729	0.497
LFFD	with CLAHE	0.671	0.743	0.682
	with colorization	0.507	0.726	0.499
	original with mask	0.492	0.703	0.496
	original without mask	0.556	0.779	0.499

The use of colorization of images to resemble images recorded in visible light has not worked for every of analyzed model. The improved metrics are noticeable for the Retina Face model and for the Ultra Light model in the RBF version (compared to the original training set). The Yolov3 model shows a similar mean average precision, regardless of the training set used, but the precision of this model is lower when used images after colorization.

Figure 4 shows the losses obtained for the training and validation sets during the transfer training of the Yolov3 model using the original set and the CLAHE data set. The loss function shown in the charts is the localization loss, which illustrates the error between the predicted boundary box and the ground truth. On the basis of these two examples, it can be seen that for the training set, both in the original set and in the CLAHE set, it decreases with successive epochs. For the validation subset of these two datasets, the loss is higher, but over the course of almost the entire learning cycle, it decreases with subsequent epochs.



**Figure 4.** Example of localization loss change during transfer learning for YOLOv3 model: (a) on the own original dataset (b) on the CLAHE dataset.

Tables 7 and 8 present the results of the measured inference time for images with two resolutions— $640 \times 480$  and  $320 \times 240$  pixels. These are two of the resolutions of the images that were collected in the created dataset. When analyzing the obtained results, it can be seen that for the Jetson Nano module, the UltraLight, RetinaFace and LFFD models achieve satisfactory inference times. The use of a relatively cheap and small module can be used when creating applications that will be used in everyday life. Compared to the measured inference time on the DGX-1 computer, the times achieved by the Jetson Nano module are very satisfactory and confirm the possibility of using this solution without large wastage of time (both for low and high resolution). The YOLOv3 model, despite achieving the best evaluation metrics, does not have the best inference time. In practical applications, models with a lower inference time will be more desirable—this will allow for faster image analysis and obtaining the result.

**Table 6.** Results obtained for testing model trained on own dataset with colorization.

Transfer Learning—Training Set with Colorization					
Model	Dataset	mAP	Precision	Recall	
UltraLight	original	0.813	0.822	0.796	
	with CLAHE	0.758	0.844	0.684	
	version-slim	with colorization	0.800	0.821	0.787
	original with mask	0.817	0.810	0.801	
	original without mask	0.810	0.843	0.790	
	original	0.833	0.815	0.795	
	with CLAHE	0.779	0.825	0.702	
	version-RBF	with colorization	0.828	0.818	0.787
	original with mask	0.831	0.800	0.800	
	original without mask	0.834	0.840	0.790	

Table 6. Cont.

Transfer Learning—Training Set with Colorization				
Model	Dataset	mAP	Precision	Recall
RetinaFace	original	0.484	0.695	0.454
	with CLAHE	0.375	0.534	0.393
	with colorization	0.468	0.702	0.438
	original with mask	0.335	0.592	0.345
	original without mask	0.687	0.807	0.644
	original	0.532	0.707	0.541
	with CLAHE	0.403	0.587	0.459
	with colorization	0.537	0.724	0.560
	original with mask	0.406	0.627	0.458
	original without mask	0.691	0.825	0.682
Yolov3	original	0.995	0.643	0.997
	with CLAHE	0.993	0.639	0.997
	with colorization	0.995	0.642	0.997
	original with mask	0.994	0.616	0.998
	original without mask	0.995	0.699	0.996
LFFD	original	0.568	0.729	0.546
	with CLAHE	0.568	0.729	0.546
	with colorization	0.665	0.733	0.667
	original with mask	0.677	0.749	0.690
	original without mask	0.682	0.794	0.589

Table 7. Inference time for images with a resolution of  $640 \times 480$ .

Inference Time in Milliseconds— $640 \times 480$ Images			
Model		Jetson Nano	DGX-1 Station
UltraLight	version-slim	28.57	5.80
	version-RBF	37.42	6.99
RetinaFace	MobileNet-0.25	37.16	29.74
	ResNet-50	58.52	20.07
Yolov3		685.11	3.82
LFFD		69.04	20.18

**Table 8.** Inference time for images with a resolution of  $320 \times 240$ .

Inference Time in Milliseconds— $320 \times 240$ Images			
	Model	Jetson Nano	DGX-1 Station
UltraLight	version-slim	34.44	7.34
	version-RBF	35.50	9.10
RetinaFace	MobileNet-0.25	35.63	9.04
	ResNet-50	57.95	15.26
	Yolov3	325.47	4.85
	LFFD	63.23	16.83

#### 4. Discussion

The use of transfer learning had a positive impact on the obtained results. For all models, they improved compared to those achieved for models trained only on the set of visible images. When analyzing the impact of preprocessing on the results obtained, the use of CLAHE also had a positive effect on the Ultra Light model in the RBF version and on the RetinaFace model with MobileNet backbone. Applying colorization to thermal images was to help check whether, for models designed to work with images made in visible light, it would help to increase the measures achieved by the models. However, it did not bring much improvement, perhaps due to the fact that the colors were not perfectly matched, many of the images were not of high quality and then the colorization was not accurate (blurred boundaries did not allow separating the entity well).

To improve the results, it would be worth considering collecting more data and training the model from scratch. In such a case, the models could achieve better parameters. Collecting only good quality data would certainly also improve the results, while in the created dataset there was both good and poor quality images (people were recorded in motion; the images had blurred edges). The prepared data set includes images of different resolutions. Certainly, the use of only high resolution images would improve the results achieved by the models.

The analyzed models were designed to operate on images recorded in visible light. In our case, we test thermal images, mostly with masked faces (92% of the images in the dataset had faces covered with masks). Using transfer learning on models that have been learned in images with uncovered faces, some of the information that is used by them (e.g., nose, mouth—characteristic features of a face) is not visible in the images from our set.

Another approach would be to create a model dedicated to face recognition in thermal images, for example based on one of the models that works well for detecting them in visible images. Adjusting and fine-tuning such a solution would certainly result in better measures achieved by the model.

The use of the dataset that was created to test this approach and creating or fine-tuning of any existing models will be applied if we use such a model in situations where people will be wearing masks (e.g., checking at the entrance to the building or in places where wearing masks is mandatory). If the model were to be more universal, more thermal images with marked faces should be collected, where people's faces are not hidden. Additionally, face detection in thermal images can be used to determine body temperature due to the benefits of thermography. This approach will be especially useful when monitoring entrances to buildings and will allow for early detection of people with increased body temperature. With this application or in crowded places, cheap and small platforms, that allow for quick image analysis combined with good precision and sensitivity achieved by the model, can be successfully used.

In [20], the authors demonstrated the possibility of using the Yolov3 model for face detection in thermal images, but without the faces with masks. They achieved an average precision on face detection of 78.5%. They also used transfer learning to adapt the Yolov3

model to work with thermographic images. In our case, the same model was also tested for use with this type of images and in our case the mAP value was higher, up to 99.3%, but we used a larger set of images. A version of the Yolov3 model with added the SE attention mechanism module and SPP module to the Yolov3 was used in [35]. The solution tested by us for the same model also achieves higher mAP values by 17.4% and 22.8% compared to the solutions proposed by the authors, even though in our case most of the faces in the images are partially covered by the virus protective mask.

In [20], authors used 5361 labelled thermal face images captured using one type of a camera. Similarly in [36] 4200 images were used to creation a database, using only one type of a camera. In our work, 7920 thermal images of a face were collected with 10,555 face labels. It is a significant contribution since it is one of the first databases that contains thermal images with faces covered by protective masks collected using four types of thermal cameras.

## 5. Conclusions

In this work, we addressed the problem of face (with protective masks) detection in thermal images. A similar problem for visible light images was well researched. The use of thermal images is very convenient for skin temperature evaluation with better privacy preservation of subjects than for visible light images (especially when defocused/smoothed images are collected). To analyze the problem, we originally collected a set of approximately 8000 images using four different thermal cameras. Each image was annotated manually and used in face detection studies. To our knowledge it is the largest set of data with the above-mentioned characteristics. We adapted and analyzed a set of face detection algorithms that proved to be efficient for visible light images. Using standard metrics, we demonstrated that the Yolov3-based model showed the best results with mAP at least 99.3%. We also presented that almost all the analyzed face detection deep models trained only on visible light images are not suitable for face with mask detection from thermal images. We showed that most of the analyzed algorithms and related data preprocessing methods require additional training using thermal datasets. Without such training, the mAP was typically less than 30%. Transfer learning significantly improved the obtained mAP values. For example, for the very time efficient UltraLight model (e.g., 35 ms per frame) the mAP improved from about 20% to about 80%. We also showed that special data preprocessing like CLAHE, false colorization, masking, etc. is not crucial to improve the precision of face detection from thermal images.

It is possible to use thermal images for face detection in conjunction with models created and trained on images recorded in visible light. The results obtained for models that have been trained only in the WIDER FACE set are much lower than in the case of using transfer learning of these models with the data collected in our own data set. Data preprocessing, such as CLAHE or image colorization, also has positive effects, depending on the model used. A model that is good at working with thermal images, even if trained only on the set of visible images, is the YOLOv3 model, which can be successfully used to work with such images.

Future work should focus on improving the algorithms to improve the precision while keeping at least the same values of mAP/recall. It will be important to extend the dataset with new images, as well as attempt to train the model from scratch, also using various types of preprocessing. Another goal should be to create a dedicated model to work with thermal images and face detection with and without masks.

**Author Contributions:** Conceptualization, N.G. and J.R.; methodology, N.G. and J.R.; software, N.G.; validation, J.R.; formal analysis, N.G.; investigation, N.G.; resources, N.G. and J.R.; data curation, N.G.; writing—original draft preparation, N.G.; writing—review and editing, J.R.; visualization, N.G.; supervision, J.R.; project administration, J.R.; funding acquisition, J.R. All authors have read and agreed to the published version of the manuscript.

**Funding:** This work has been partially supported by subsidy Funds of Electronics, Telecommunications and Informatics Faculty, Gdansk University of Technology. The models were trained and tested using NVIDIA DGX-1, supported by Polish Ministry of Science and Higher Education under the grant 6950/II-KDM/SP/2019.

**Institutional Review Board Statement:** The experiment was performed with permission of local Committee for Ethics of Research with Human Participants of 02.03.2021.

**Informed Consent Statement:** Informed consent was obtained from all subjects involved in the study.

**Acknowledgments:** We would like to thank Mariusz Kaczmarek for their help with data acquisition.

**Conflicts of Interest:** The authors declare no conflict of interest.

## References

1. Kwaśniewska, A.; Rumiński, J.; Rad, P. Deep features class activation map for thermal face detection and tracking. In Proceedings of the 2017 10th International Conference on Human System Interactions (HSI), Ulsan, Korea, 17–19 July 2017; pp. 41–47.
2. Wu, Z.; Peng, M.; Chen, T. Thermal face recognition using convolutional neural network. In Proceedings of the 2016 International Conference on Optoelectronics and Image Processing (ICOIP), Warsaw, Poland, 10–12 June 2016; pp. 6–9.
3. Ruminski, J.; Nowakowski, A.; Kaczmarek, M.; Hryciuk, M. Model-based parametric images in dynamic thermography. *Pol. J. Med. Phys. Eng.* **2000**, *6*, 159–164.
4. Sonkusare, S.; Ahmedt-Aristizabal, D.; Aburn, M.J.; Nguyen, V.T.; Pang, T.; Frydman, S.; Denman, S.; Fookes, C.; Breakspear, M.; Guo, C.C. Detecting changes in facial temperature induced by a sudden auditory stimulus based on deep learning-assisted face tracking. *Sci. Rep.* **2019**, *9*, 1–11. [[CrossRef](#)] [[PubMed](#)]
5. Ruminski, J.; Kwasniewska, A. Evaluation of respiration rate using thermal imaging in mobile conditions. In *Application of Infrared to Biomedical Sciences*; Springer Nature: Singapore, 2017; pp. 311–346.
6. Rumiński, J. Analysis of the parameters of respiration patterns extracted from thermal image sequences. *Biocybern. Biomed. Eng.* **2016**, *36*, 731–741. [[CrossRef](#)]
7. Kwasniewska, A.; Ruminski, J.; Szankin, M.; Kaczmarek, M. Super-resolved thermal imagery for high-accuracy facial areas detection and analysis. *Eng. Appl. Artif. Intell.* **2020**, *87*, 103263. [[CrossRef](#)]
8. Kwasniewska, A.; Szankin, M.; Ruminski, J.; Sarah, A.; Gamba, D. Improving Accuracy of Respiratory Rate Estimation by Restoring High Resolution Features With Transformers and Recursive Convolutional Models. In Proceedings of the IEEE/CVF Conference on Computer Vision and Pattern Recognition, Nashville, TN, USA, 19–25 June 2021; pp. 3857–3867.
9. Reese, K.; Zheng, Y.; Elmaghraby, A. A comparison of face detection algorithms in visible and thermal spectrums. In Proceedings of the Int'l Conference on Advances in Computer Science and Application, Amsterdam, The Netherlands, 7–8 June 2012.
10. Friedrich, G.; Yeshurun, Y. Seeing people in the dark: Face recognition in infrared images. In *International Workshop on Biologically Motivated Computer Vision*; Springer: Cham, Switzerland, 2002; pp. 348–359.
11. Viola, P.; Jones, M.J. Robust real-time face detection. *Int. J. Comput. Vis.* **2004**, *57*, 137–154. [[CrossRef](#)]
12. Zhang, S.; Zhu, X.; Lei, Z.; Shi, H.; Wang, X.; Li, S.Z. FaceBoxes: A CPU real-time face detector with high accuracy. In Proceedings of the 2017 IEEE International Joint Conference on Biometrics (IJCB), Denver, CO, USA, 1–4 October 2017; pp. 1–9.
13. Yang, W.; Jiachun, Z. Real-time face detection based on YOLO. In Proceedings of the 2018 1st IEEE International Conference on Knowledge Innovation and Invention (ICKII), Jeju, Korea, 23–27 July 2018; pp. 221–224.
14. Yang, S.; Luo, P.; Loy, C.C.; Tang, X. Wider face: A face detection benchmark. In Proceedings of the IEEE Conference on Computer Vision and Pattern Recognition, Las Vegas, NV, USA, 27–30 June 2016; pp. 5525–5533.
15. Pang, L.; Ming, Y.; Chao, L. F-DR Net: Face detection and recognition in One Net. In Proceedings of the 2018 14th IEEE International Conference on Signal Processing (ICSP), Beijing, China, 12–16 August 2018; pp. 332–337.
16. Hussain, S.; Yu, Y.; Ayoub, M.; Khan, A.; Rehman, R.; Wahid, J.A.; Hou, W. IoT and Deep Learning Based Approach for Rapid Screening and Face Mask Detection for Infection Spread Control of COVID-19. *Appl. Sci.* **2021**, *11*, 3495. [[CrossRef](#)]
17. Kopaczka, M.; Nestler, J.; Merhof, D. Face Detection in Thermal Infrared Images: A Comparison of Algorithm- and Machine-Learning-Based Approaches. In *Advanced Concepts for Intelligent Vision Systems*; Springer: Cham, Switzerland, 2017; pp. 518–529.
18. Dalal, N.; Triggs, B. Histograms of Oriented Gradients for Human Detection. *Comput. Vis. Pattern Recognit.* **2005**, *1*, 886–893.
19. Redmon, J.; Farhadi, A. Yolov3: An incremental improvement. *arXiv* **2018**, arXiv:1804.02767.
20. Silva, G.; Monteiro, R.; Ferreira, A.; Carvalho, P.; Corte-Real, L. Face Detection in Thermal Images with YOLOv3. In *International Symposium on Visual Computing*; Springer: Cham, Switzerland, 2019; pp. 89–99.
21. Szegedy, C.; Vanhoucke, V.; Ioffe, S.; Shlens, J.; Wojna, Z. Rethinking the inception architecture for computer vision. In Proceedings of the IEEE Conference on Computer Vision and Pattern Recognition, Las Vegas, NV, USA, 27–30 June 2016; pp. 2818–2826.
22. Peng, M.; Wang, C.; Chen, T.; Liu, G. NIRFaceNet: A Convolutional Neural Network for Near-Infrared Face Identification. *Information* **2016**, *7*, 61. [[CrossRef](#)]
23. Szegedy, C.; Liu, W.; Jia, Y.; Sermanet, P.; Reed, S.; Anguelov, D.; Erhan, D.; Vanhoucke, V.; Rabinovich, A. Going deeper with convolutions. In Proceedings of the 2015 IEEE Conference on Computer Vision and Pattern Recognition (CVPR), Boston, MA, USA, 7–12 June 2015; pp. 1–9.

24. Krizhevsky, A.; Sutskever, I.; Hinton, G.E. ImageNet Classification with Deep Convolutional Neural Networks. In *Advances in Neural Information Processing Systems*; Pereira, F., Burges, C.J.C., Bottou, L., Weinberger, K.Q., Eds.; Curran Associates, Inc.: New York, NY, USA, 2012; Volume 25, pp. 1097–1105.
25. Li, S.Z.; Chu, R.; Liao, S.; Zhang, L. Illumination Invariant Face Recognition Using Near-Infrared Images. *IEEE Trans. Pattern Anal. Mach. Intell.* **2007**, *29*, 627–639. [[CrossRef](#)] [[PubMed](#)]
26. Sayed, M.; Baker, F. Thermal Face Authentication with Convolutional Neural Network. *J. Comput. Sci.* **2018**, *14*, 1627–1637. [[CrossRef](#)]
27. Nikisins, O.; Nasrollahi, K.; Greitans, M.; Moeslund, T.B. RGB-D-T Based Face Recognition. In Proceedings of the 2014 22nd International Conference on Pattern Recognition, Stockholm, Sweden, 24–28 August 2014; pp. 1716–1721.
28. Su, J.W.; Chu, H.K.; Huang, J.B. Instance-aware image colorization. In Proceedings of the IEEE/CVF Conference on Computer Vision and Pattern Recognition, Seattle, WA, USA, 13–19 June 2020; pp. 7968–7977.
29. Ultra-Lightweight Face Detection Model. Available online: <https://github.com/Linzaer/Ultra-Light-Fast-Generic-Face-Detector-1MB> (accessed on 5 January 2021).
30. Deng, J.; Guo, J.; Yuxiang, Z.; Yu, J.; Kotsia, I.; Zafeiriou, S. RetinaFace: Single-stage Dense Face Localisation in the Wild. *arXiv* **2019**, arXiv:1905.00641.
31. RetinaFace in PyTorch. Available online: [https://github.com/biubug6/Pytorch\\_Retinaface](https://github.com/biubug6/Pytorch_Retinaface) (accessed on 10 January 2021).
32. He, Y.; Xu, D.; Wu, L.; Jian, M.; Xiang, S.; Pan, C. LFFD: A Light and Fast Face Detector for Edge Devices. *arXiv* **2019**, arXiv:1904.10633.
33. Schütze, H.; Manning, C.D.; Raghavan, P. *Introduction to Information Retrieval*; Cambridge University Press: Cambridge, UK, 2008; Volume 39.
34. Powers, D.M. Evaluation: From precision, recall and F-measure to ROC, informedness, markedness and correlation. *arXiv* **2020**, arXiv:2010.16061.
35. Li, D.; Zhu, X.; Chen, X.; Tian, D.; Hu, X.; Qin, G. Thermal Imaging Face Detection Based on Transfer Learning. In Proceedings of the 2021 6th International Conference on Smart Grid and Electrical Automation (ICSGEA), Kunming, China, 29–30 May 2021; pp. 263–266.
36. Mallat, K.; Dugelay, J.L. A benchmark database of visible and thermal paired face images across multiple variations. In Proceedings of the 2018 International Conference of the Biometrics Special Interest Group (BIOSIG), Darmstadt, Germany, 26–28 September 2018; pp. 1–5.

